





Assembly and photocatalysis of three novel metal–organic frameworks tuned by metal polymeric motifs

Lei Wang, Yuexia Shan, Xiaomin Gu, Liang Ni & Wenli Zhang

To cite this article: Lei Wang, Yuexia Shan, Xiaomin Gu, Liang Ni & Wenli Zhang (2015) Assembly and photocatalysis of three novel metal–organic frameworks tuned by metal polymeric motifs, *Journal of Coordination Chemistry*, 68:11, 2014–2028, DOI: [10.1080/00958972.2015.1035652](https://doi.org/10.1080/00958972.2015.1035652)



To link to this article: <http://dx.doi.org/10.1080/00958972.2015.1035652>

 View supplementary material 

 Accepted author version posted online: 30 Mar 2015.
Published online: 12 May 2015.

 Submit your article to this journal 

 Article views: 83

 View related articles 

 View Crossmark data 

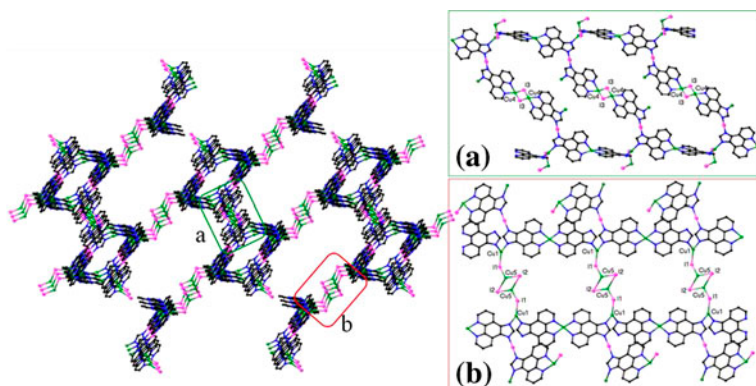


Assembly and photocatalysis of three novel metal–organic frameworks tuned by metal polymeric motifs

LEI WANG*, YUEXIA SHAN, XIAOMIN GU, LIANG NI and WENLI ZHANG

School of Chemistry and Chemical Engineering, Jiangsu University, Zhenjiang, PR China

(Received 20 November 2014; accepted 11 March 2015)



The 3D structure of **3** connected by $(\text{CuI})_2$ (a) or $(\text{ICuI})_2$ (b) unit

By using a thiodiacetate, phenanthroline, and tuning the metal salts in the reaction system, three new metal–organic coordination complexes, $\{[\text{Co}(\text{MOPIP})_2(\text{tda})] \cdot \text{H}_2\text{O}\}_{1/2}$ (**1**), $[\text{Cd}(\text{MOPIP})_2(\text{tda})]_2 \cdot 3\text{H}_2\text{O}$ (**2**), and $[\text{Cu}_5\text{I}_4(\text{MOPIP})_3 \cdot \text{H}_2\text{O}]_n$ (**3**) (tda = $\text{S}(\text{CH}_2\text{COO})_2^{2-}$, thiodiacetate; MOPIP = 2-(4-methoxyphenyl)-1*H*-imidazo[4,5-*f*][1, 10]phenanthroline), have been prepared through hydrothermal reactions. In **1** and **2**, the metal ($\text{Co}^{2+}/\text{Cd}^{2+}$) centers are connected by tda to form a mononuclear molecule, which connect to a two-dimensional (2-D) layer by $\text{N} \cdots \text{H} \cdots \text{O}$ hydrogen bonds. By selecting the copper iodide salt we get **3**, where the Cu^+ center exhibits three different coordination types, which has never been seen before in the same compound, and linked by iodide and MOPIP to construct a new 3-D framework. Compound **3** represents the first example of MOPIP showing a new coordination mode with four nitrogens all coordinated. The metal salts play an important role in assembly of the structures of **1**–**3**. Introduction of MOPIP shows significant effect on the dimensionalities of complexes. The fluorescence and catalytic properties of **1** and **3** have also been investigated.

Keywords: Hydrothermal synthesis; Crystal structure; Fluorescence; Catalytic properties; Thiodiacetate

*Corresponding author. Email: wanglei86@ujs.edu.cn

1. Introduction

Crystal engineering of metal complexes has developed, especially coordination polymers. The structures of coordination polymers could be effectively influenced by factors such as the coordination of metal ions, solvent system [1], ligands [2], templates [3], counterions [4], non-covalent interactions [5], etc. 1,10-Phenanthroline and its derivatives are used in coordination polymers due to their strong chelating abilities and good π -conjugation, usually as terminal ligands. Herein, we use 2-(4-methoxyphenyl)-1*H*-imidazo-[4,5-*f*][1, 10] phenanthroline (MOPIP) as the ligand. It contains an extended imidazo-ring with two nitrogens, which can provide supramolecular interactions (in **1** and **2**), and also provide lone pair electrons to connect metal or halides forming a multidimensional structure in **3**.

The study of the thiodiacetate (tda) transition metal chemistry was initiated several decades ago. It has a polycarboxylate structure, but also a versatile complexing agent with potential hard (O carboxyl) and soft (S thioether) donors, giving various binding modes to hard, soft or intermediate metal ions. Tda displays a variety of coordination modes [6]: (a) chelating *fac*-SO₂-tridentate (group I); (b) *fac*-SO₂-tridentate chelating role + μ -carboxylato bridging (group II); (c) head-to-tail carboxylate–carboxylate bridging modes without metal–sulfur bond (group III); (d) S,O-bidentate chelating, with a free acid S-carboxymethyl arm (group IV). The thiodiacetate is a flexible polydentate ligand which provides two carboxylate groups connected with the same metal in our work.

Three transition metal–organic coordination polymers, $\{[\text{Co}(\text{MOPIP})_2(\text{tda})]\cdot\text{H}_2\text{O}\}_{1/2}$ (**1**), $[\text{Cd}(\text{MOPIP})_2(\text{tda})]_2\cdot 3\text{H}_2\text{O}$ (**2**), and $[\text{Cu}_5\text{I}_4(\text{MOPIP})_3]_n$ (**3**), have been hydrothermally synthesized and structurally characterized. In addition, the luminescence of these compounds has also been discussed.

2. Experimental

2.1. General materials and methods

The neutral chelating ligand MOPIP was synthesized according to the literature method [7]. Other reagents for synthesis were purchased from commercial sources and used as received. Transmission mode FT-IR spectra were obtained as KBr pellets between 400 and 4000 cm^{-1} using a Nicolet Nexus 470 infrared spectrometer. Elemental analysis was carried out with a Perkin-Elmer 240C analyzer. Thermogravimetric analysis (TG) was performed on a Germany Netzsch STA449C at a heating rate of 10 $^{\circ}\text{C}\cdot\text{min}^{-1}$ in nitrogen. Fluorescence measurement was carried out at room temperature with a Cary Eclipse spectrometer.

2.2. Syntheses of compounds

2.2.1. $\{[\text{Co}(\text{MOPIP})_2(\text{tda})]\cdot\text{H}_2\text{O}\}_{1/2}$ (1**).** A mixture of $\text{Co}(\text{NO}_3)_2\cdot 6\text{H}_2\text{O}$ (0.073 g, 0.25 mmol), tda (0.075 g, 0.41 mmol), MOPIP (0.082 g, 0.25 mmol), NaOH (0.004 g, 0.1 mmol), and H_2O (18 mL) was placed in a 25 mL Teflon-lined stainless steel vessel under autogenous pressure at 165 $^{\circ}\text{C}$ for 5 days. After cooling to room temperature, red block crystals of **1** (0.083 g) were collected by filtration and washed with distilled water in 76% yield (based on MOPIP). Anal Calcd (%) for $\text{C}_{44}\text{H}_{30}\text{N}_8\text{O}_7\text{SCo}$: C, 60.47; H, 3.46; N, 12.83. Found

(%): C, 60.46; H, 3.48; N, 12.82. IR (KBr): $\nu = 3447(\text{m}), 2934(\text{m}), 2834(\text{m}), 1609(\text{m}), 1520(\text{s}), 1399(\text{m}), 1357(\text{m}), 1307(\text{m}), 1178(\text{m}), 1071(\text{m}), 837(\text{m}), 734(\text{m}), 515(\text{w})$.

2.2.2. $[\text{Cd}(\text{MOPIP})_2(\text{tda})]_2 \cdot 3\text{H}_2\text{O}$ (2**).** A mixture of $\text{Cd}(\text{OAc})_2 \cdot 2\text{H}_2\text{O}$ (0.067 g, 0.25 mmol), tda (0.045 g, 0.25 mmol), MOPIP (0.082 g, 0.25 mmol), NaOH (0.004 g, 0.1 mmol), and H_2O (18 mL) was placed in a 25 mL Teflon-lined stainless steel vessel under autogenous pressure at 165 °C for 5 days. After cooling to room temperature, red block crystals of **2** (0.070 g) were collected by filtration and washed with distilled water in 60% yield (based on MOPIP). Anal Calcd (%) for $\text{C}_{88}\text{H}_{62}\text{N}_{16}\text{O}_{15}\text{S}_2\text{Cd}_2$: C, 56.44; H, 3.34; N, 11.97. Found (%): C, 56.43; H, 3.36; N, 11.96. IR (KBr): $\nu = 3448(\text{m}), 2930(\text{m}), 2836(\text{m}), 1609(\text{m}), 1521(\text{s}), 1397(\text{m}), 1357(\text{m}), 1304(\text{m}), 1177(\text{m}), 1069(\text{m}), 829(\text{m}), 741(\text{m}), 515(\text{w})$.

2.2.3. $[\text{Cu}_5\text{I}_4(\text{MOPIP})_3 \cdot \text{H}_2\text{O}]_n$ (3**).** Compound **3** was also synthesized by using a method similar to that described for synthesis of **1** except that CuI (0.095 g, 0.5 mmol) was used instead of $\text{Co}(\text{NO}_3)_2 \cdot 6\text{H}_2\text{O}$ (0.073 g, 0.25 mmol). Red block crystals of **3** (0.093 g) were collected by filtration and washed with distilled water in 52% yield (based on Cu). Anal Calcd for $\text{C}_{60}\text{H}_{33}\text{N}_{12}\text{O}_3\text{I}_4\text{Cu}_5$: C, 40.14; H, 1.86; N, 9.36. Found: C, 40.13; H, 1.88; N, 9.35%. IR (KBr): $\nu = 3732(\text{m}), 3436(\text{m}), 3243(\text{m}), 1612(\text{m}), 1521(\text{s}), 1452(\text{m}), 1401(\text{s}), 1310(\text{m}), 1250(\text{m}), 1180(\text{m}), 879(\text{m}), 809(\text{s}), 551(\text{w}), 513(\text{w}), 411(\text{w})$.

2.3. Catalysis experiments

The photocatalytic activity of **1** and **3** was tested by degradation of methyl orange under visible-light irradiation. The experiments were performed at room temperature as follows: 16 mg of sodium persulfate and 13.1 mg of **1** (26.6 mg of **3**) was added to 80 mL of methyl orange solution ($10 \text{ mg} \cdot \text{L}^{-1}$) in a Pyrex reactor. The pH of the dispersion was adjusted to 3 with sulfuric acid (1 M) and exposed to visible-light irradiation under stirring. At given time intervals, the suspension was centrifuged to remove the remnant photocatalyst from the liquid. The concentrations of methyl orange were monitored by checking the absorbance at 506 nm using a UV-2450 (Shimadzu) spectrophotometer.

2.4. Crystal data collection and refinement

Single-crystal X-ray data of all compounds were collected at room temperature with a Bruker SMART Apex CCD diffractometer with MoK_α radiation ($\lambda = 0.71073 \text{ \AA}$) at 293(2) K using ω -scan mode. The structures were solved by direct methods with SHELXS-97 [8] and refined by SHELXL-97 [9] using full-matrix least-squares techniques on F^2 . All non-hydrogen atoms were easily found from the difference Fourier map and refined anisotropically, and hydrogens were generated geometrically and added to the structure factor calculation. The crystallographic data and structure refinement parameters for the compounds are summarized in table 1. Selected bond lengths and angles are listed in tables S1–S3 (see online supplemental material at <http://dx.doi.org/10.1080/00958972.2015.1035652>).

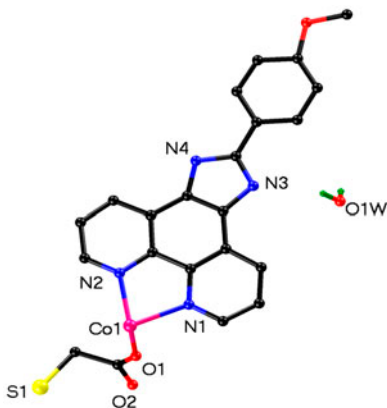
Table 1. Crystal data and structure refinement for **1–3**.

Compound	1	2	3
Empirical formula	C ₄₄ H ₃₄ N ₈ O ₇ SCo	C ₈₈ H ₅₈ N ₁₆ O ₁₅ S ₂ Cd ₂	C ₆₀ H ₃₉ N ₁₂ O ₆ I ₄ Cu ₅
Formula weight (g mol ⁻¹)	877.78	1868.42	1801.38
μ (MoK α) (mm ⁻¹)	0.575	0.663	3.966
Crystal size (mm)	0.2 \times 0.2 \times 0.2	0.2 \times 0.2 \times 0.2	0.2 \times 0.2 \times 0.2
Crystal system	Monoclinic	Triclinic	Triclinic
Space group	<i>C2/c</i>	<i>P-1</i>	<i>P-1</i>
<i>a</i> (Å)	16.329(3)	10.019(2)	13.623(3)
<i>b</i> (Å)	10.273(2)	17.503(3)	15.411(3)
<i>c</i> /Å	23.051(5)	23.159(5)	15.489(3)
α (°)	90	77.85(3)	75.88(3)
β (°)	101.29(3)	89.00(3)	67.98(3)
γ (°)	90	87.03(3)	81.67(3)
Volume (Å ³)	3791.9(13)	3964.8(13)	2918.4(10)
<i>Z</i>	4	4	1
Limiting indices	$-20 \leq h \leq 17$ $-12 \leq k \leq 7$ $-24 \leq l \leq 28$	$-11 \leq h \leq 12$ $-21 \leq k \leq 21$ $-28 \leq l \leq 28$	$-16 \leq h \leq 13$ $-16 \leq k \leq 18$ $-19 \leq l \leq 18$
<i>T</i> (K)	293(2)	293(2)	293(2)
<i>F</i> (0 0 0)	1812	1728	1728
θ range for data collection (°)	3.61–26.02	3.04–26.02	3.04–26.04
Calculated density (mg·cm ⁻³)	1.538	1.476	2.050
<i>R</i> _{int}	0.0558	0.0000	0.0645
GO _F	1.017	0.992	1.111
<i>R</i> 1, <i>wR</i> 2 [<i>I</i> > 2 σ (<i>I</i>)]	0.0715, 0.1329	0.1348, 0.3137	0.1101, 0.3001
Reflections collected/unique	9332/3630	14,792/14,792	27,386/11,099

3. Results and discussion

3.1. Description of crystal structure

3.1.1. Crystal structure of [Co(MOPIP)₂(tda)]·H₂O (1). The X-ray single-crystal structure determination of **1** suggested that it crystallized in the monoclinic system with *C2/c* space group. Compound **1** consists of one Co(II), two MOPIP ligands, one tda

Figure 1a. The molecular structure of **1**. All hydrogens are omitted for clarity.

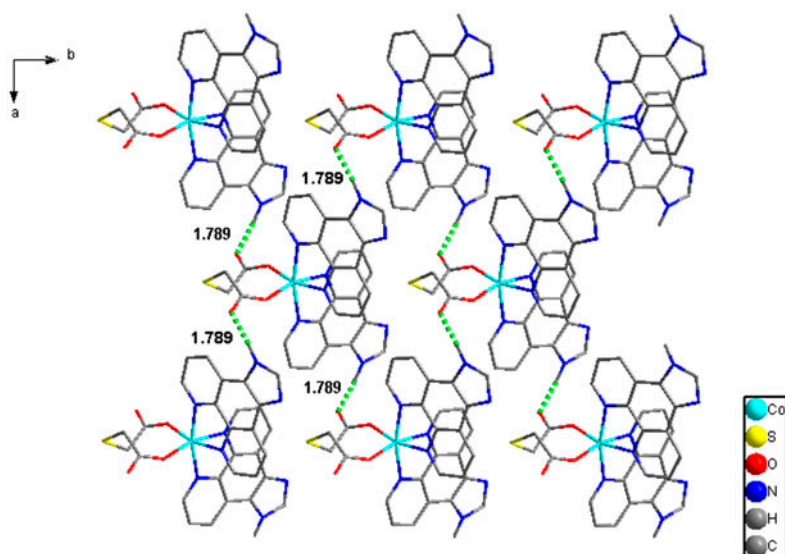


Figure 1b. 2-D layer structure of **1** connected by N–H···O hydrogen bonds.

anion, and one uncoordinated water. As depicted in figure 1(a), Co1 is six-coordinate and surrounded by four nitrogens (N1, N2, N1A, and N2A) from two MOPIP ligands and two oxygens (O1 and O1A) from different carboxyl groups of one tda. Water O1w is disordered over two positions with the same occupancy of 50% [10].

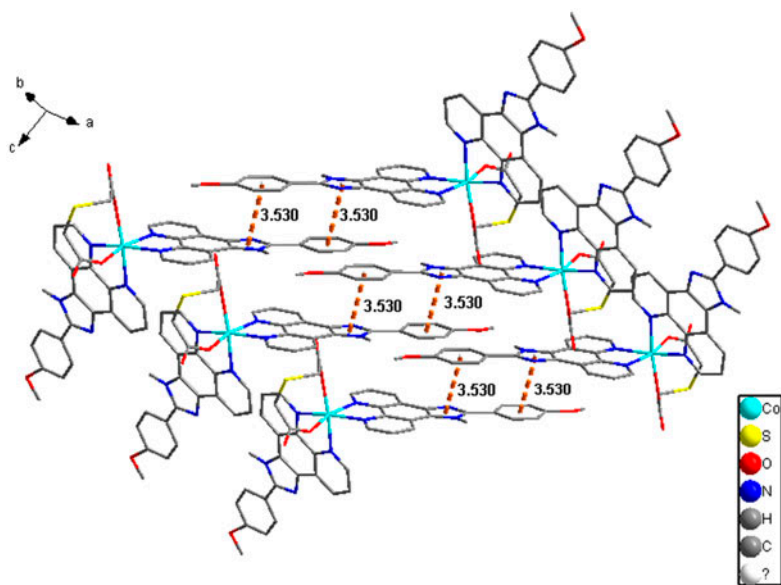


Figure 1c. π – π stacking interactions between neighboring layers of **1**.

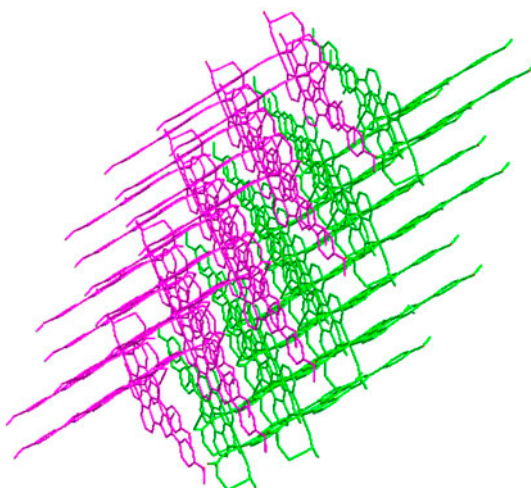
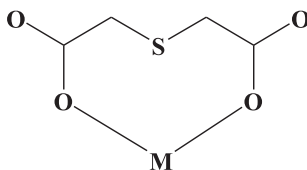


Figure 1d. Three-dimensional supramolecular packing structures of **1**.

In **1**, both carboxyl groups of tda are monodentate and connect the same Co(II) (scheme 1) to form a mononuclear structure. The MOPIP ligands are H-donors to form intermolecular hydrogen bonding interactions with uncoordinated O from tda [N4–H1C···O2A]. Hydrogen bonding interactions result in the formation of a 2-D supramolecular network [figure 1(b)]. The [N4–H1C···O2A] distance of 1.789 Å falls in the normal N–H···O hydrogen bond range from 1.72 to 1.99 Å [11]. Compound **1** exhibits face-to-face π – π stacking interactions between imidazole and benzene rings of two different MOPIP ligands in adjacent 2-D layers [figure 1(c)]. The distances of centroid–centroid are 3.530 Å. Therefore, adjacent layers are further interconnected via intermolecular π – π stacking interactions to form a 3-D supramolecular structure [figure 1(d)].

3.1.2. Crystal structure of [Cd(MOPIP)₂(tda)]₂·3H₂O (2**).** Compound **2** was crystallized in the triclinic system with *P*-1 space group. There are two Cd(MOPIP)₂(tda) subunits and three uncoordinated waters as depicted in figure 2. Compounds **1** and **2** are isostructural and therefore only the structure of **1** is described in detail.

3.1.3. Crystal structure of [Cu₅I₄(MOPIP)₃·H₂O]_n (3**).** The X-ray crystal structure of **3** is depicted in figure 3(a). The asymmetric unit of **3** consists of five Cu ions, four iodides,



Scheme 1. Coordination mode of tda in **1**.



Downloaded by [Mizoram University] at 14:34 28 December 2015

Downloaded by [Mizoram University] at 14:34 28 December 2015

Downloaded by [Mizoram University] at 14:34 28 December 2015



Downloaded by [Mizoram University] at 14:34 28 December 2015

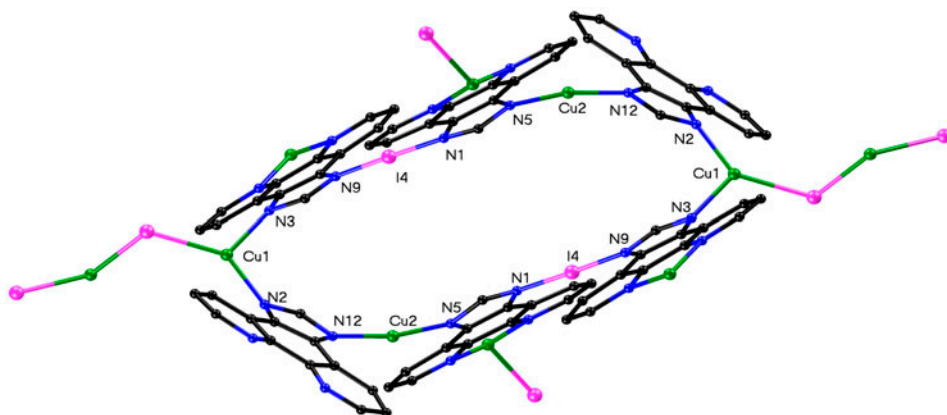


Figure 3b. The 18-membered macrometallocycle of **3**; the methoxyphenyl was omitted for clarity.

ions, two Cu2 ions, two I4 ions, and twelve nitrogens from the imidazole rings of six MOPIP ligands. Each 18-membered macrometallocycle connects by Cu3 forming a straight chain [figure 3(c)] and each chain connects to the adjacent by the unit of $(\text{I3Cu4})_2$ [figure 3(d)] to form a two-dimensional plane. The distance of Cu4-I3 is from 2.561(2) to 2.609(2) Å. The $(\text{I1Cu5I2})_2$ units link adjacent planes to the 3-D framework [figure 3(e)]. The packing organization reveals that the 3-D framework is arranged parallel to each other [figure 3(f)] because of the C–H···I atypical hydrogen bonds (table S5).

3.2. FT-IR analysis

The FT-IR spectrum of **1** (similar to **2**) revealed the presence of vibrationally active carboxylate groups. Antisymmetric stretches $\nu_{\text{as}}(\text{COO}^-)$ for the carboxylate carbonyls appeared at 1520 cm^{-1} , symmetric vibrations $\nu_{\text{s}}(\text{COO}^-)$ for the same groups appeared at 1399 cm^{-1} . The frequencies shifted to lower values in comparison to the corresponding vibrations in free tda due to the connection with cobalt. The band at 439 cm^{-1} for **1** indicates that the metal ions are coordinated with oxygen. Meanwhile, the band corresponding to pyridine

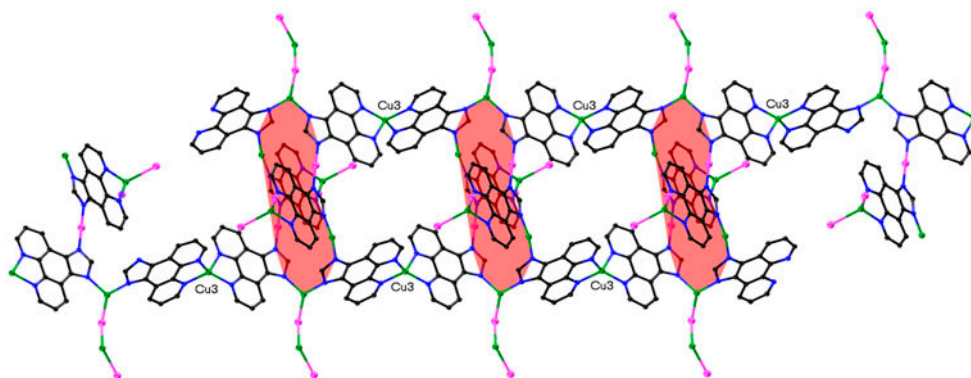


Figure 3c. One-dimensional chain structure formed by Cu3 with the macrometallocycle (filled with pink); the methoxyphenyl was omitted for clarity (see <http://dx.doi.org/10.1080/00958972.2015.1035652> for color version).

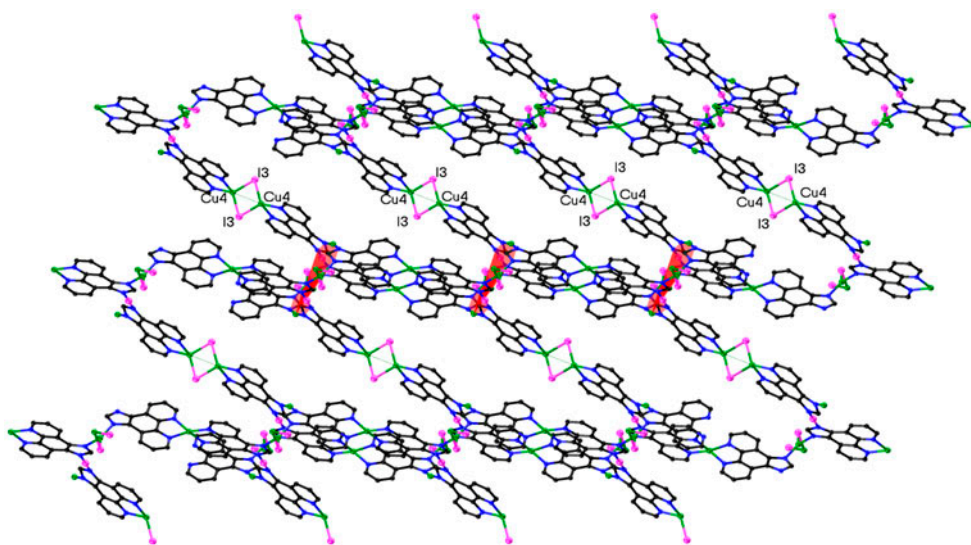


Figure 3d. Two-dimensional structure formed by $(\text{Cu}_4\text{I}_3)_2$ unit with the 1-D chain; the methoxyphenyl was omitted for clarity.

ring vibrations $\nu_{\text{C}=\text{N}}$ of the ligands MOPIP shift to lower wavenumber of 1520 cm^{-1} for **1** (1521 cm^{-1} for **3**); this negative shift indicates coordination of pyridine nitrogen to the metal [12]. The signal at 515 cm^{-1} for **1** (513 cm^{-1} for **3**) also proves coordination of metal ions and nitrogen [13]. The broad bands at $3447\text{--}3436\text{ cm}^{-1}$ are attributed to vibrations of water.

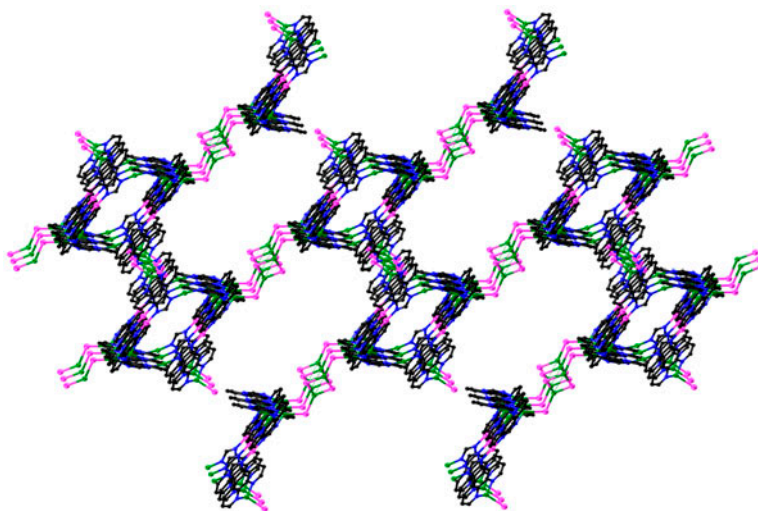


Figure 3e. The three-dimensional supramolecular packing structures of **3**; the methoxyphenyl was omitted for clarity.

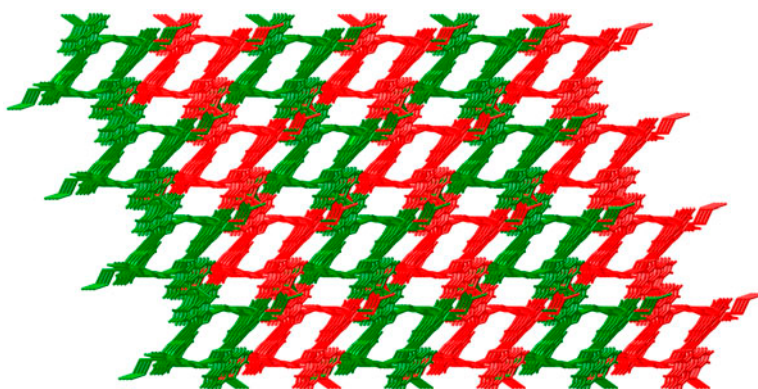
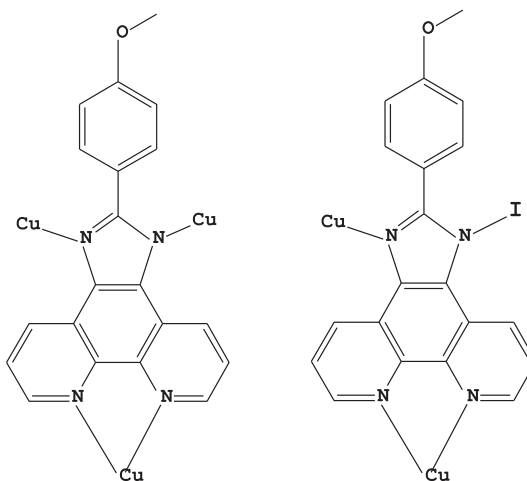


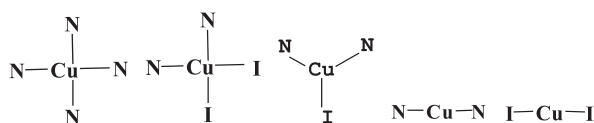
Figure 3f. The AB packing of the 3-D framework; the methoxyphenyl was omitted for clarity.

3.3. Thermal property

Thermal stabilities of **1–3** were determined by using a thermogravimetric (TG) analyzer (figure 4). Compound **1** shows a three-step weight loss. The first weight loss of 1.88% (Calcd 1.97%) occurs from 100 to 314 °C, which corresponds to loss of water. The second weight loss of 17.95% (Calcd 19.99%) occurs from 350 to 423 °C, which corresponds to



Scheme 2. Coordination mode of MOPIP in **3**.



Scheme 3. Coordination mode and environment of Cu ion.

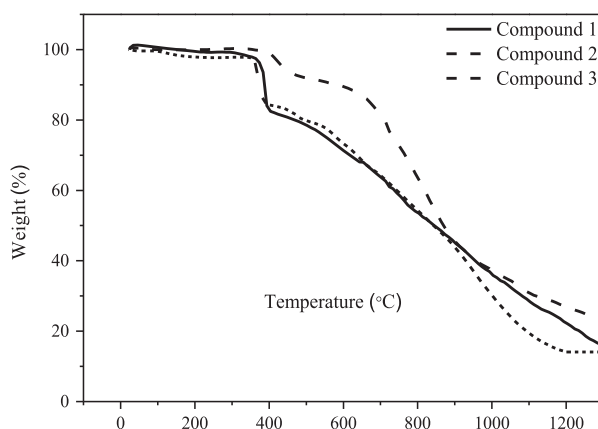


Figure 4. TG curve of **1–3**.

loss of one tda per formula unit. The last weight loss of 65.17% (Calcd 69.54%) between 450 and 1250 °C is ascribed to loss of two-coordinated MOPIP ligands. After decomposition, the final product may be CoO. The thermal stability of **2** is similar to **1**. The first weight loss of 2.34% (Calcd 2.89%) corresponds to loss of water. The second sharp weight loss of 16.59% (Calcd 16.11%) corresponds to release of one equivalent of tda per formula unit. The third loss of 66.91% (Calcd 70.5%) after 463 °C is ascribed to loss of MOPIP ligands, with CdO forming as the final remnant. Compound **3** is stable until 363 °C and the first weight loss of 1.17% (Calcd 1.36%) is ascribed to loss of water. The packing structure collapses after 413 °C; the weight loss of 76.06% (Calcd 76.74%) may correspond to decomposition of MOPIP and sublimation of iodine. The weight losses are in agreement with the theoretical volume of the crystal structure, with CuO formed as the final remnant. Thermal analysis reveals that **1–3** are stable to 350, 361, and 413 °C, respectively.

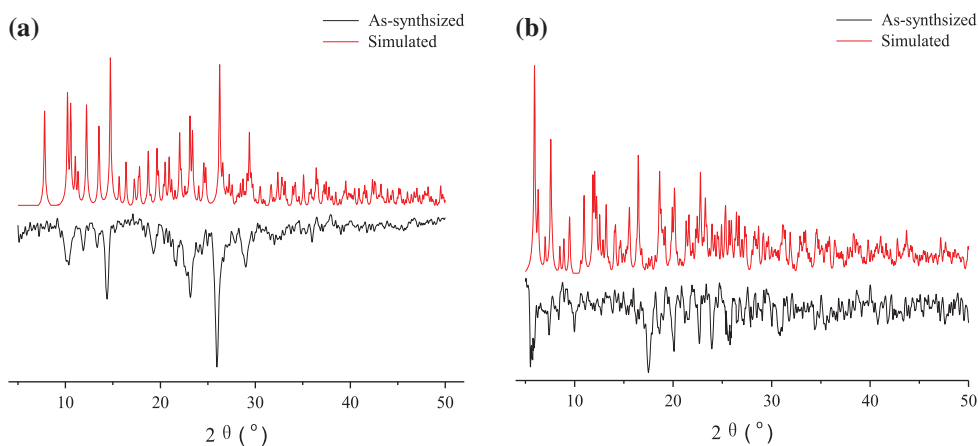


Figure 5. Comparison of PXRD patterns of the simulated pattern from the single-crystal structure determination and the as-synthesized products in **1** (a) and **3** (b).

3.4. Powder X-ray diffraction analyses

The powder X-ray diffraction (PXRD) experiments of **1** and **3** were performed to confirm the phase purity of those bulk materials. As shown in figure 5, the experimental PXRD patterns almost correspond with the computer-simulated from the single-crystal data for the compounds, indicating the purity of the synthesized compounds. The differences of reflection intensities between the simulated and the experimental pattern may be caused by preferred orientation of the powder [14].

3.5. Fluorescent analysis

The solid-state fluorescence spectra of **1** and **3** at room temperature were recorded (figure 6). Free MOPIP displays two main emissions at 380 and 469 nm upon excitation at 292 nm, assigned to $\pi \rightarrow \pi^*$ transitions [15]. Free tda displays main emission bands at 450 and 469 nm upon excitation at 300 nm [16], attributed to $\pi^* \rightarrow n$ transitions. Compound **1** exhibits two strong peaks at 392 and 470 nm due to MOPIP ligands and weak emission at 452 due to the tda ($\lambda_{\text{ex}} = 300$ nm). The small red shift emission peaks probably are related to the intraligand fluorescent emission [17–19]. For **3**, the emission peaks at 453 and 471 nm ($\lambda_{\text{ex}} = 348$ nm) are assigned to MOPIP and the weak emission of 549 nm may be attributed to ligand-to-metal charge transfer [20]. Thus, **1** and **3** will be potential photoluminescent materials.

3.6. Catalytic properties

Methyl orange has been widely used in printing, textile, paper, pharmaceutical industries, and other fields [21]. It is an acidic/anionic dye potentially harmful to the environment [22]. Methyl orange was chosen as an organic pollutant to evaluate the photocatalytic efficiency of the compounds as heterogeneous catalysts, with sodium persulfate added as oxidant [23]. The possible catalytic mechanism has been reported [24]. In the absence of the catalyst, a solution of methyl orange mixed with $\text{Na}_2\text{S}_2\text{O}_8$ is stable (the degradation efficiency was only 8.9%), which indicates that there is no obvious reaction taking place between methyl orange and $\text{Na}_2\text{S}_2\text{O}_8$ (figure 7). However, when **1** or **3** was added, the mixture activates

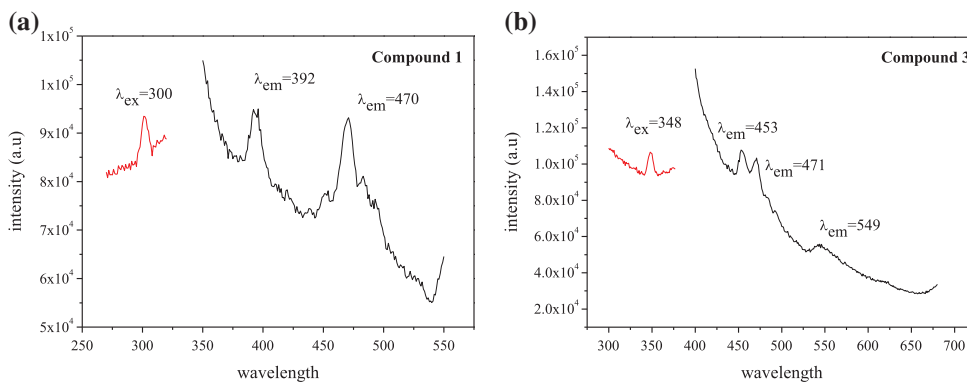


Figure 6. Solid-state fluorescent spectra of **1** (a) and **3** (b).

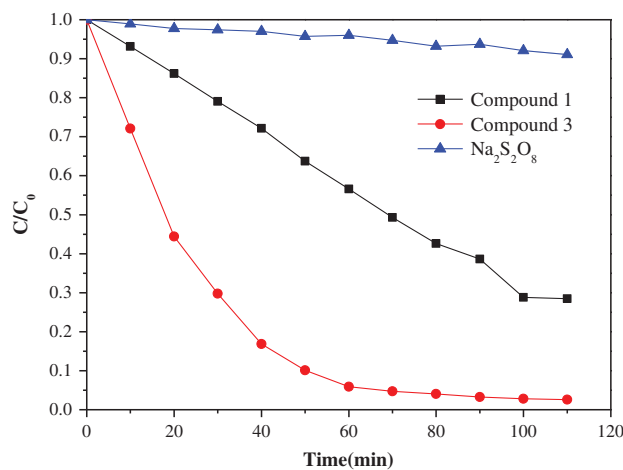


Figure 7. Degradation of methyl orange.

$\text{S}_2\text{O}_8^{2-}$ reaction with methyl orange solution and leads to color removal of the dye. Compound **3** has higher activity for the degradation than **1** (figure 7). The degradation of methyl orange in **1** was 71.2% after 100 min and nearly ceased with time (figure 8), while the degradation of methyl orange in **3** was close to 95% after 70 min (figure 9).

To investigate the kinetics of methyl orange photocatalytic degradation by **1** and **3** mixed with $\text{Na}_2\text{S}_2\text{O}_8$, experimental data can be described by the Langmuir–Hinshelwood model [25] as expressed by $\ln(C/C_0) = -kt$ (k = apparent reaction rate constant). C_0 is the initial concentration of methyl orange, t is the reaction time, and C is the concentration of methyl orange at the reaction time t . As shown in figure 10, the plot of $\ln(C_0/C)$ and irradiation time (t) is approximately linear and approximated the first-order kinetic equation. The

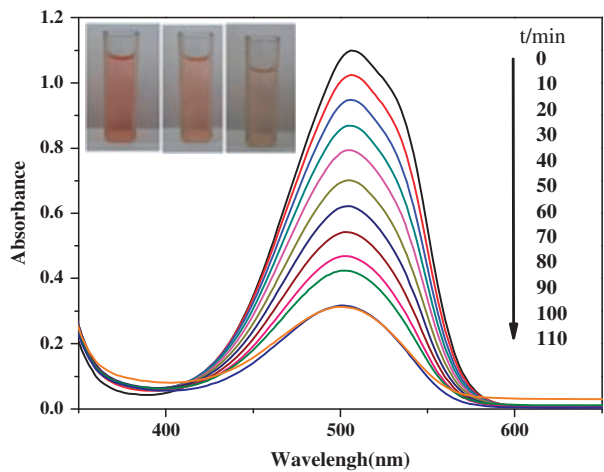


Figure 8. The photocatalytic degradation of methyl orange by **1**.

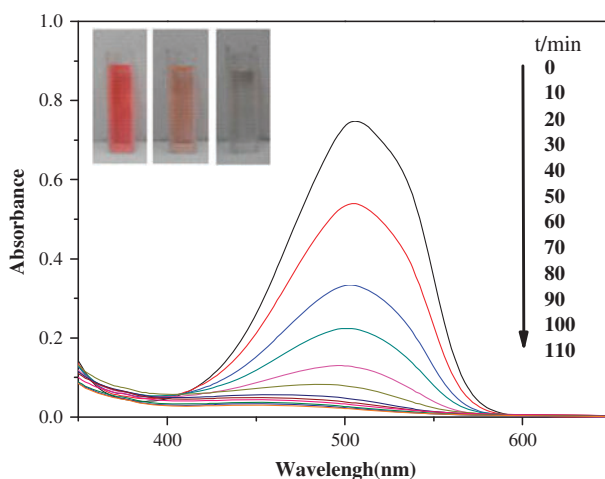


Figure 9. The photocatalytic degradation of methyl orange by **3**.

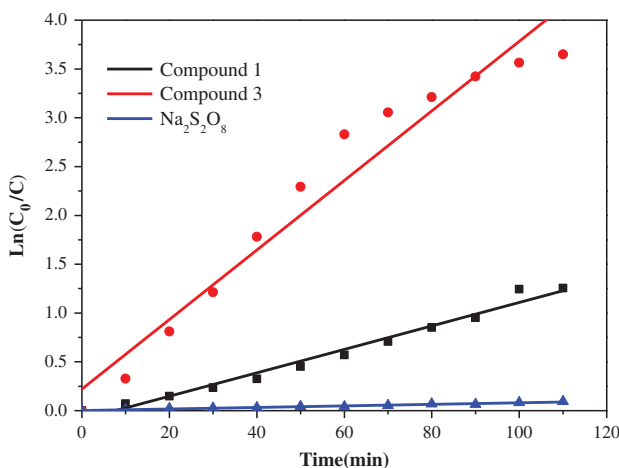


Figure 10. Photocatalytic degradation kinetics of methyl orange by **1** or **3** and $\text{Na}_2\text{S}_2\text{O}_8$.

calculated apparent rate constant k value for **3** ($k = 2.1378 \text{ h}^{-1}$) is about 2.96 times higher than that of **1** ($k = 0.7206 \text{ h}^{-1}$) and much higher than for $\text{Na}_2\text{S}_2\text{O}_8$ ($k = 0.0473 \text{ h}^{-1}$). So, **1** and **3** could be chosen as photocatalyst to degrade methyl orange.

4. Conclusion

Three coordination polymers have been obtained under hydrothermal conditions. Compounds **1** and **2** are zero-dimensional structures similarly and exhibit 2-D layers owing to hydrogen bonds and extend to 3-D supramolecular structures by π - π stacking interactions. Unlike **1** and **2**, **3** has a 3-D packing structure connected by $(\text{CuI})_2$ or $(\text{ICuI})_2$ unit.

Compounds **1** and **3** are potential photocatalytic materials due to thermal stability and catalytic properties.

Disclosure statement

No potential conflict of interest was reported by the authors.

Funding

This work was supported by the Programs of Senior Talent Foundation of Jiangsu University [grant number 14JDG053]; Jiangsu Postdoctoral Science Foundation [grant number 1401176C].

References

- [1] C.B. Liu, S.S. Wang, G.B. Che, H. Zhao, W.W. Li, X.Y. Li, Z.L. Xu. *Inorg. Chem. Commun.*, **27**, 69 (2013).
- [2] X.L. Wang, Y.F. Bi, H.Y. Lin, G.C. Liu. *Cryst. Growth Des.*, **7**, 6 (2007).
- [3] Y. Chen, Y.C. Ma, S.M. Chen. *Cryst. Growth Des.*, **13**, 4154 (2013).
- [4] M. Ángeles Vázquez-Fernández, M. Isabel Fernández-García, A.M. González-Noya, M. Maneiro, M.R. Bermejo, M. Jesús Rodríguez-Doutón. *Polyhedron*, **31**, 379 (2012).
- [5] X.J. Gao, S.W. Jin, L. Jin, X.H. Ye, L. Zheng, J.W. Li, B.P. Jin, D.Q. Wang. *J. Mol. Struct.*, **1075**, 384 (2014).
- [6] C. Alarcón-Payer, T. Pivetta, D. Choquesillo-Lazarte, J.M. González-Pérez, G. Crisponi, A. Castiñeiras, J. Nicolás-Gutiérrez. *Inorg. Chim. Acta*, **358**, 1918 (2005).
- [7] G.B. Che, S.S. Wang, X.L. Zha, X.Y. Li, C.B. Liu, X.J. Zhang, Z.L. Xu, Q.W. Wang. *Inorg. Chim. Acta*, **394**, 481 (2013).
- [8] G.M. Sheldrick. *SHELXS-97, Program for Solution of Crystal Structures*, University of Göttingen, Göttingen (1997).
- [9] G.M. Sheldrick. *SHELXL-97, Program for Refinement of Crystal Structures*, University of Göttingen, Göttingen (1997).
- [10] Z.Y. Shi, X.J. Gu, J. Peng, E.B. Wang. *J. Mol. Struct.*, **737**, 147 (2005).
- [11] G.A. Jeffrey. *Crystallogr. Rev.*, **9**, 135 (2003).
- [12] S. Prasanna, B.R. Bijini, K. Rajendra Babu, S.M. Eapen, M. Deepa, C.M.K. Nair. *J. Cryst. Growth*, **333**, 36 (2011).
- [13] L. Wang, L. Ni, J. Yao. *Solid State Sci.*, **14**, 1361 (2012).
- [14] W.W. Shan, S.S. Ma, H.L. Wang, H.H. Li, R.J. Meng, C.Z. Mei. *J. Inorg. Organomet. Polym. Mater.*, **24**, 468 (2014).
- [15] L. Wang, L. Ni, J. Yao. *Polyhedron*, **59**, 115 (2013).
- [16] C. Gabriel, C.P. Raptopoulou, A. Terzis, V. Psycharis, F. Gul-E-Noor, M. Bertmer, C. Mateescu, A. Salifoglou. *Cryst. Growth Des.*, **13**, 2573 (2013).
- [17] X. Shi, G.S. Zhu, Q.R. Fang, G. Wu, G. Tian, R.W. Wang, D.L. Zhang, M. Xue, S.L. Qiu. *Eur. J. Inorg. Chem.*, **1**, 185 (2004).
- [18] K.J. Wei, Y.S. Xie, J. Ni, M. Zhang, Q.L. Liu. *Cryst. Growth Des.*, **6**, 1341 (2006).
- [19] K.J. Wei, J. Ni, Y.S. Xie, Q.L. Liu. *Inorg. Chem. Commun.*, **10**, 279 (2007).
- [20] Y.Q. Sun, J. Hu, H.H. Zhang, Y.P. Chen. *J. Solid State Chem.*, **186**, 189 (2012).
- [21] E. Haque, J.E. Lee, I.T. Jang, Y.K. Hwang, J.S. Chang, J. Jegal, S.H. Jung. *J. Hazard. Mater.*, **181**, 535 (2010).
- [22] Y.J. Li, X.D. Li, J.W. Li, J. Yin. *Water Res.*, **40**, 1119 (2006).
- [23] L. Qin, S.L. Xiao, P.J. Ma, G.H. Cui. *Transition Met. Chem.*, **38**, 627 (2013).
- [24] Z.Q. Feng, X.L. Yang, Y.F. Ye. *J. Inorg. Organomet. Polym. Mater.*, **24**, 684 (2014).
- [25] A.K. Sajjad, S. Shamaila, B.Z. Tian, F. Chen, J.L. Zhang. *J. Hazard. Mater.*, **177**, 781 (2010).